

PFC/JA-87-25

Experimental Studies of Divertor Stabilization
in an Axisymmetric Tandem Mirror

J.A. Casey, B.G. Lane, J.H. Irby, K.L. Brau,
S.N. Golovato, W.C. Guss, J. Kesner, R.S. Post,
E. Sevillano, and J. Zielinski.

December 1987

Plasma Fusion Center
Massachusetts Institute of Technology
Cambridge, Massachusetts 02139 USA

This work was supported by the Department of Energy under contract number DE-AC02-78ET51013. Reproduction, translation, publication, use and disposal, in whole or part, by or for the United States government is permitted.

Submitted for publication in: *The Physics of Fluids*

Abstract

A divertor coil set has been installed on the Tara tandem mirror for stabilization of $m = 1$ flute-like modes. We discuss the effectiveness of divertor stabilization in experiments where $m = 1$ modes are driven to instability by plug electron cyclotron heating (ECH) in an ion cyclotron heated (ICH) plasma. The instability onset is characterized by thresholds in ECH power, fueling rate, ICH power and mapping radius of the divertor null. In general, the stability is enhanced by mapping the null radially inwards into the plasma. The interdependence of these parameters and their effect on equilibrium profiles and stability boundaries are discussed.

I – INTRODUCTION

Recent designs for mirror confinement devices have attempted to obtain as much axisymmetry as possible within the constraint of stability to interchange modes^{1,2}. Tara^{3,4} and other tandem mirror experiments (TMX-U⁵, Phaedrus⁶, Gamma-10⁷) have used non-axisymmetric minimum- B field configurations to provide MHD stability at the expense of power consumption, access to the plasma, and transport due to ion drifts across flux surfaces⁸.

We have installed a magnetic divertor coil set in the Tara central cell for halo fueling^{9,10} and axisymmetric stabilization of interchange modes^{11,12}. In this paper we report on the stabilization of rigid flute-like modes during divertor operation in an axisymmetric field configuration. This instability occurs in these experiments during fundamental electron cyclotron heating (ECH) in one of the axisymmetric plug cells adjacent to the central cell, although it can also be initiated by other power sources or adjustment of input gas pressure or central cell Ion Cyclotron Heating (ICH) power. We find that the threshold for instability occurs at higher ECH power levels during divertor operation.

When driven to instability, the plasma is best described by a rigid gaussian profile rotating azimuthally around the machine axis¹³. The

transition between this behavior and quiescent operation is quite sudden. We describe here the parameterization of the thresholds for loss of stability. The range of conditions for which stable operation is possible is enhanced significantly by operation of the divertor, and scales with the strength of the divertor field.

The structure of this paper is as follows: In section II we briefly describe the divertor coil set and operation. In section III we discuss the theoretical reasons which motivated the installation of the magnetic divertor. In section IV we review the nature of the mode under consideration as seen in Tara. In section V we discuss the dependence of stability on key operating parameters. In section VI we discuss the qualitative agreement of results with theory, and several alternative mechanisms which may explain the stabilization. In section VII we summarize our conclusions.

II – Divertor Construction and Operation

The magnetic geometry of Tara is shown in figure 1. The axisymmetric central cell (10 m long) is bounded by axisymmetric plug cells, which in turn are bounded by minimum- B anchors. In these

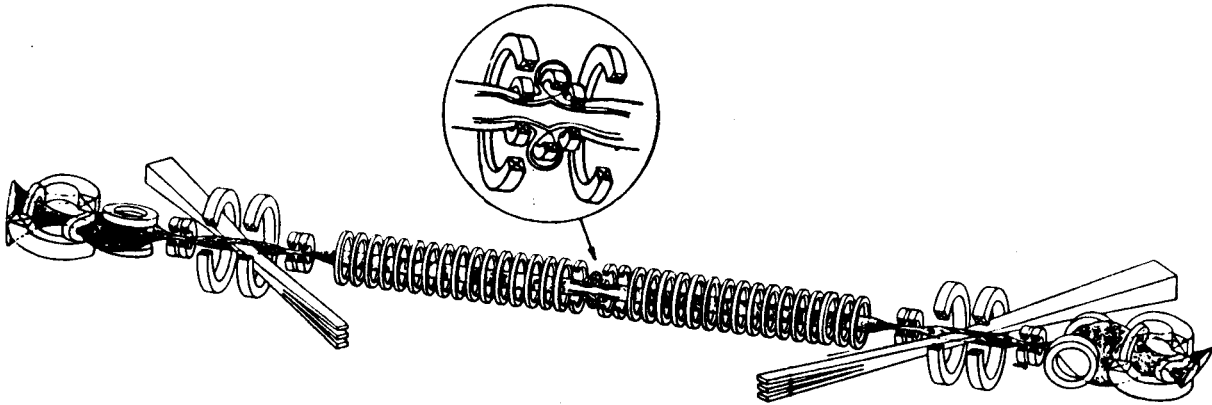


Figure 1. Schematic of the Tara experiment, showing coil set, flux tube, and axicell neutral beam injection. The divertor coil set is highlighted.

experiments, the anchor magnets were energized only to preserve flux mapping to the endwalls for diagnostic purposes. No supplementary ion or electron heating was energized in the anchor cells, thus plasma streamed through without the stabilizing effect of enhancing global β weighted curvature¹⁴.

The central cell is constructed with a magnetic field “bump” at the midplane for fueling and ICH heating. For one meter to either side of the central cell midplane, the magnetic field is raised to 4.6 kGauss from a value of 2.6 kGauss in either side (the “wells”). A gas box here provides the primary fueling source for the plasma discharge, and is constructed of two fast time-response piezo-electric gas injectors and

a series of close fitting limiters¹⁰. ICH slow waves are launched from an antenna at the “bump”, and propagate to either side where heating occurs at the ion cyclotron resonance in the “well”. This arrangement has the advantage that the hot mirror trapped ions in the “well” are isolated from charge-exchange losses they would undergo in the gas box region¹⁵.

The divertor coil set is located in the center of the “bump”, between the gas box and the ICH antenna. The coil set, shown in figures 1 and 2, consists of three coils internal to the vacuum chamber, which replace one of the original external central cell coils. Two of these (the “boost coils”) are run in the same sense as the central cell coil set in order to prop up the local field and localize the region of reduced field. The center (“bucking”) coil is run in the opposite sense of the other coils to divert flux around itself and create a null in the shape of an azimuthal ring between the three coils. It is predicted that stability occurs via azimuthal currents in the null “shorting out” radial perturbations of the plasma column.

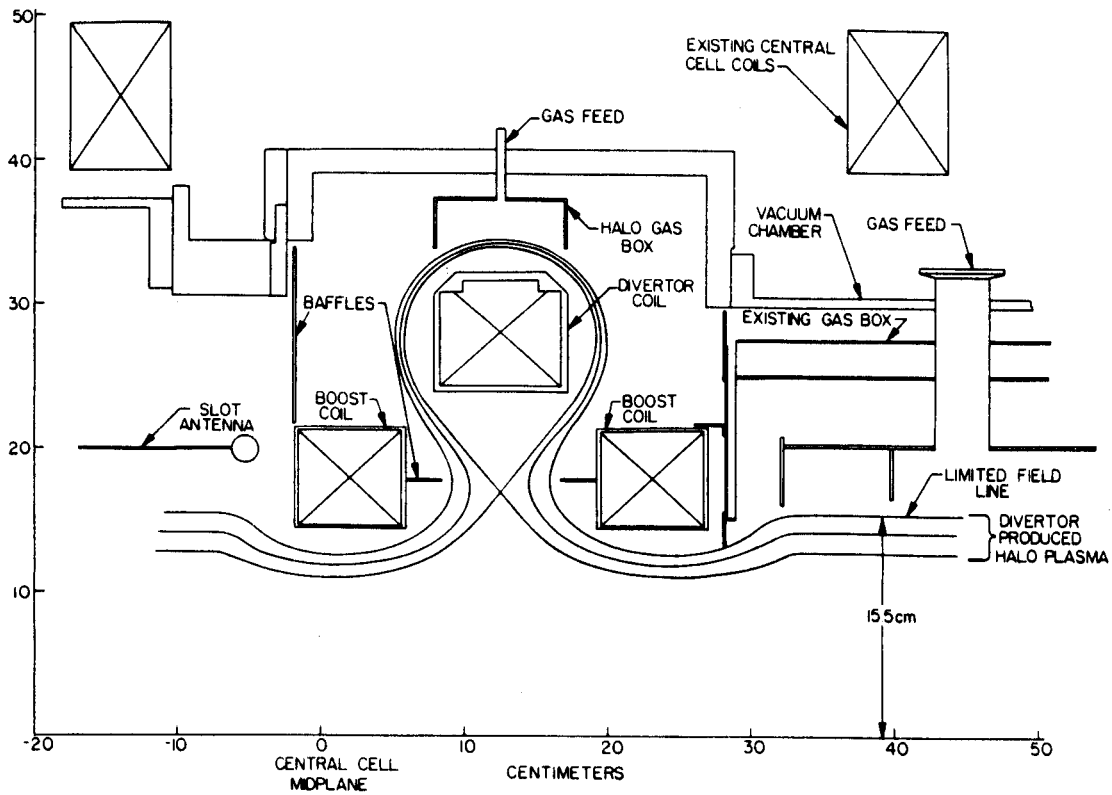


Figure 2. Schematic of the Tara divertor. The three coil divertor, central cell and halo gas boxes, and slot ICH antenna are shown.

Confinement in the diverted flux will be poorer than on the adjacent flux which maps just inside the separatrix. Scrape-off losses from limiters and the coil supports must be refueled from the gas box or reflux, and power losses for refueling and charge-exchange over this extra flux path must be compensated. The bucking coil is thus held in place by thin (3.2mm) spokes, and the power and cooling feed-through cross-sections are carefully designed to minimize scrape-off in divertor

mode. The divertor was installed on the magnetic “bump”, like the gas box, to minimize resultant charge-exchange cooling of the hot mirror trapped ions in the central cell “well”.

The divertor coil can be run in non-divertor mode (where the bucking coil is not energized and the small coils are only partially energized to avoid scrape-off), or divertor mode (where a fraction of the Tara flux is mapped around the bucking coil). In divertor mode, the coil currents can be adjusted to vary the mapping of diverted flux. Although the null always resides close to the same location, the mapped radius of the null flux tube in the central cell “well” varies with the divertor currents. In typical operation, the boost coils are kept at constant current and the bucking coil is varied to change this mapping. The operating range of the bucking coil spans null radii mapped to the central cell “well” from the limiter edge (19 cm) to 14.5 cm. This corresponds to diverting 0% to 40% of the central cell flux around the bucking coil.

III – Theoretical Predictions for the Magnetic Divertor

A theoretical treatment¹¹ of the divertor magnetic geometry has predicted that MHD frequency modes must exhibit a node at the flux

surface containing the null. This results comes about for the following reason: electrons that pass within an electron gyroradius of the null become trapped and stream around the ring null before re-emerging at a random azimuthal angle (but on the same flux tube). A localized electron perturbation would thus spread within a wave period over the entire flux surface that mapped to within an electron gyro-radius of the null, giving rise to an adiabatic electron response. Ions on the same flux tube would $\mathbf{E} \times \mathbf{B}$ drift in the perturbed electric fields of the wave as usual, since the majority of the ions trapped in the “wells” on either side of the magnetic plateau do not feel the effects of the null during a perturbation wave period. Ions that do traverse the null have their pitch angle scattered but do not drift azimuthally appreciably during a single traversal. The combination of adiabatic electron response and $\mathbf{E} \times \mathbf{B}$ ion response will only support waves at drift wave frequencies. The response of the perturbation (driven by the core pressure gradient) however, is that of a higher frequency MHD wave. MHD frequency waves will not satisfy quasineutrality at the flux surface of the null, thus the radial mode structure of the MHD wave must exhibit a node at this flux surface. Finite Larmor radius (FLR) effects act to stabilize a radial perturbation which is not rigid, thus the vanishing of the mode at the null flux tube induces FLR stabilization. The stability of

the plasma is determined by the competition between MHD, rotational drives and FLR stabilization. Numerical analysis of the linear eigenmode equations leads to the conclusion that stability depends on the ion pressure gradient at the null flux surface, since it is at this point where the FLR effects are weakest. This predicts therefore, that the coherent bulk fluctuations of the plasma will be strongly damped at the null flux tube, provided an ion pressure gradient is maintained on the null flux surface.

There are several alternate stabilization mechanisms that are possible: 1) compressibility due to the large local curvature in the null region^{16,17}, 2) line-tying on the divertor coils or limiters^{18,19}, and 3) modification of the edge pressure profile in such a way that the equilibrium shifts towards stability or ponderomotive stabilization is enhanced. None of these alternative explanations may be entirely discounted. We will discuss them further in section VI.

IV – Nature of Dominant Low Frequency Instability in Tara

We characterize the stability related plasma parameters primarily by using diagnostics which yield radial profile information. In this

way, we observe equilibrium changes in the radial density profile width, shape, and peak as well as bulk motion of the plasma column itself. The major tools used for this are: 1) a five-chord interferometer array in the central cell, 2) an eight-chord light detector array on the north end of the central cell, and 3) an eight-detector Faraday cup array at the south endwall. All of these arrays look at the up-down orientation of the plasma column.

The interferometer array data is de-convolved to fit an elliptic Gaussian profile rotating around an offset center of motion²⁰. The fit optimizes values for peak density, $1/e$ width, ellipticity, offset, and $m = 1$ mode amplitude, frequency and phase for each time “window” (typically several MHD periods long) during the shot. For comparisons of centroid motion to the diagnostics below, a simplified fit (no ellipticity or rotation) finds peak density, $1/e$ radius, and centroid position at higher time resolution, (i.e. faster than the unstable mode period). The Faraday cup signals, (proportional to central cell density weighted by parallel and radial confinement times), are similarly fit to a Gaussian profile at each time point. The light signals (called the Plasma Position Detector, or PPD) for these experiments were filtered to select visible continuum light at 3435\AA , assumed to originate

from molecular radiation and/or Bremsstrahlung, and also analyzed for Gaussian width and centroid.

The centroid positions of these arrays (mapped back to the central cell “well”) typically track one another very well¹³. The dominant characteristics of the coherent mode as seen in Tara are: (a) low frequency 3-15 kHz; (b) axially flute-like; (c) radially coherent. The data leading to these conclusions are summarized in figure 3 which shows a single off-axis interferometer signal versus time, and the positions of the centroids for a Gaussian fitted to the interferometer, PPD and end-loss array. In this case the instability is well developed. The flute-like nature of the mode is clear as well as the agreement in the maximum displacement of the centroid from the machine axis. Closer inspection of the interferometer signals shows the radial coherence of the mode — the oscillation is quite smooth and repeatable with no evidence for filamentation or other higher order structure. It is typical that the instability does not grow until the plasma extinguishes on the limiters, but saturates at a finite amplitude.

V – Parameter dependence of the instability

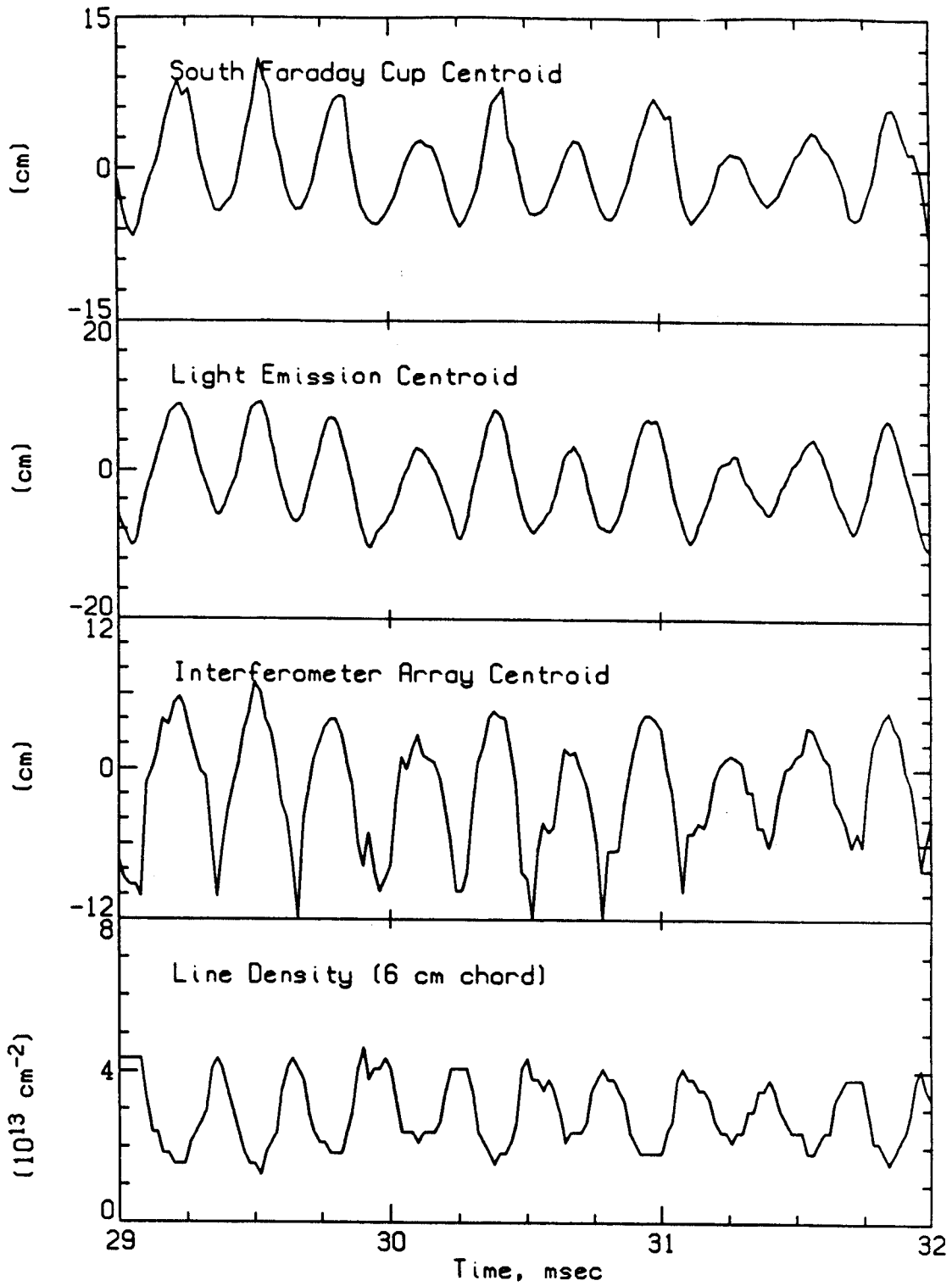


Figure 3. During the $m = 1$ instability, the flute-like nature of the mode is demonstrated in the coherence of the centroid of oscillation as measured in widely different locations and on different diagnostics. The centroid is measured at the south fan Faraday cup array, the PPD (plasma position detector) light detector array in the north end of the central cell, and at the multi-chord interferometer array in the south "well" of the central cell.

A variety of variables determine the plasma stability. These include axial and radial density and temperature profiles, magnetic geometry, geometry of metal limiters, ICH wave field profiles, distribution of neutral gas through the plasma and impurities. Since all these are not controllable in the experiment, we concentrate instead on operational parameters which are directly controllable but which change a number of factors at once. We will examine the stability of the plasma as a function of ECH power resonant at 10 kG in one of the axisymmetric end cells, current in the bucking coil (i.e. null radius), central cell ICH power, and gas fueling rate.

In figure 4 we show the fluctuation amplitude variation for a series of shots in which the ECH power in one of the axisymmetric plug cells was scanned. We note that the instability has a sharp threshold behavior with respect to ECH power. Below a particular power the plasma is quiescent and the fluctuation level is independent of ECH power. Above this level fluctuations are large, but again the power dependence is weak. We interpret this behavior as evidence of a stability boundary.

We can raise the ECH power level at which instability appears by increasing the bucking coil current, placing the null deeper into the

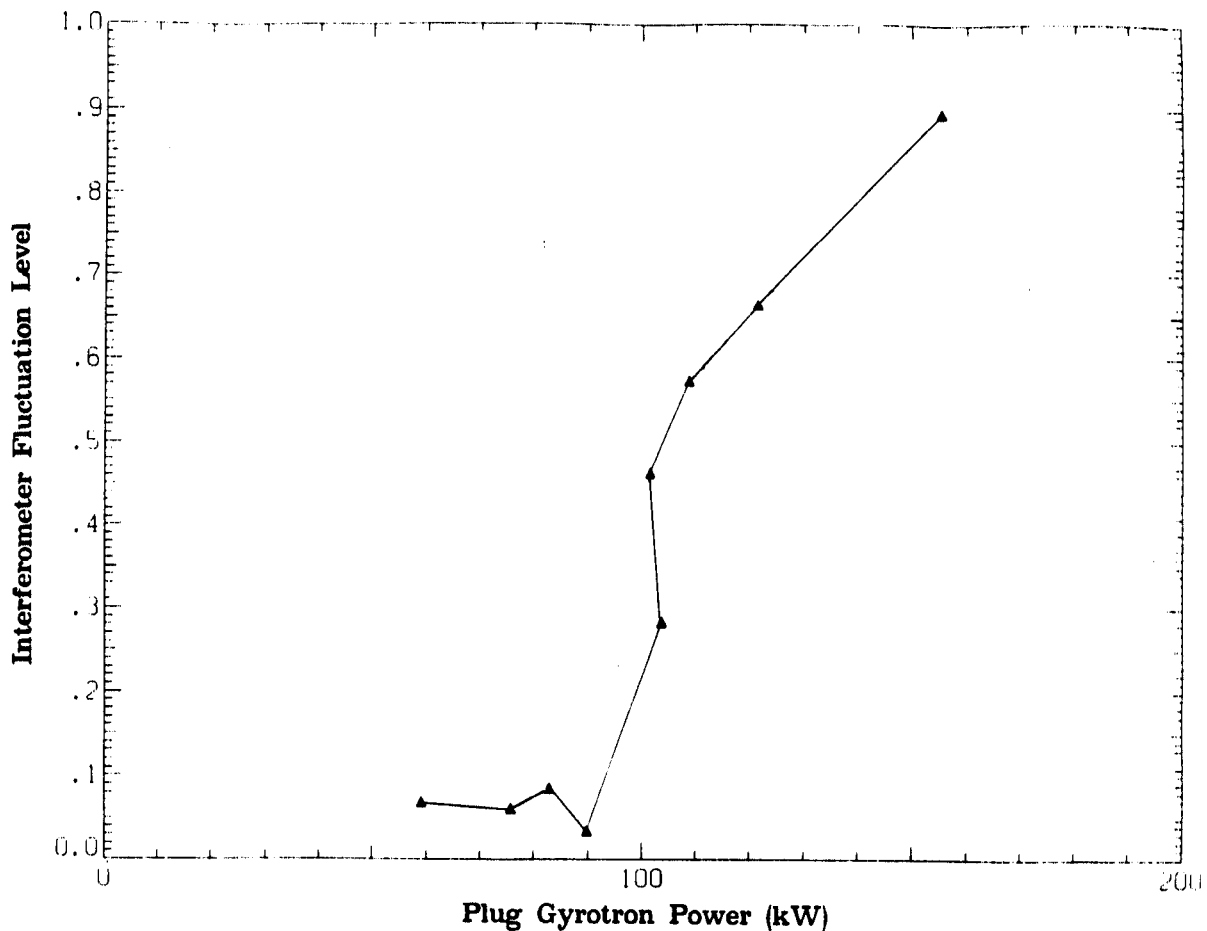


Figure 4. The stability threshold is shown as the north axicell plug ECH power is increased. The fluctuations are measured as $\delta n/n$ on a central cell interferometer.

plasma (on a larger pressure gradient). We can similarly enhance the stability by increasing the ICH power level. (Slow wave ICH has been shown to be stabilizing on Tara¹⁴, presumably via ponderomotive forces²¹.) Figure 5 shows the time history of a shot in which the ICH power is ramped down during the course of the shot. At $t = 40 - 42$ msec, the plasma undergoes a transition to instability. This behavior is repeatable, and correlates with ICH power level rather

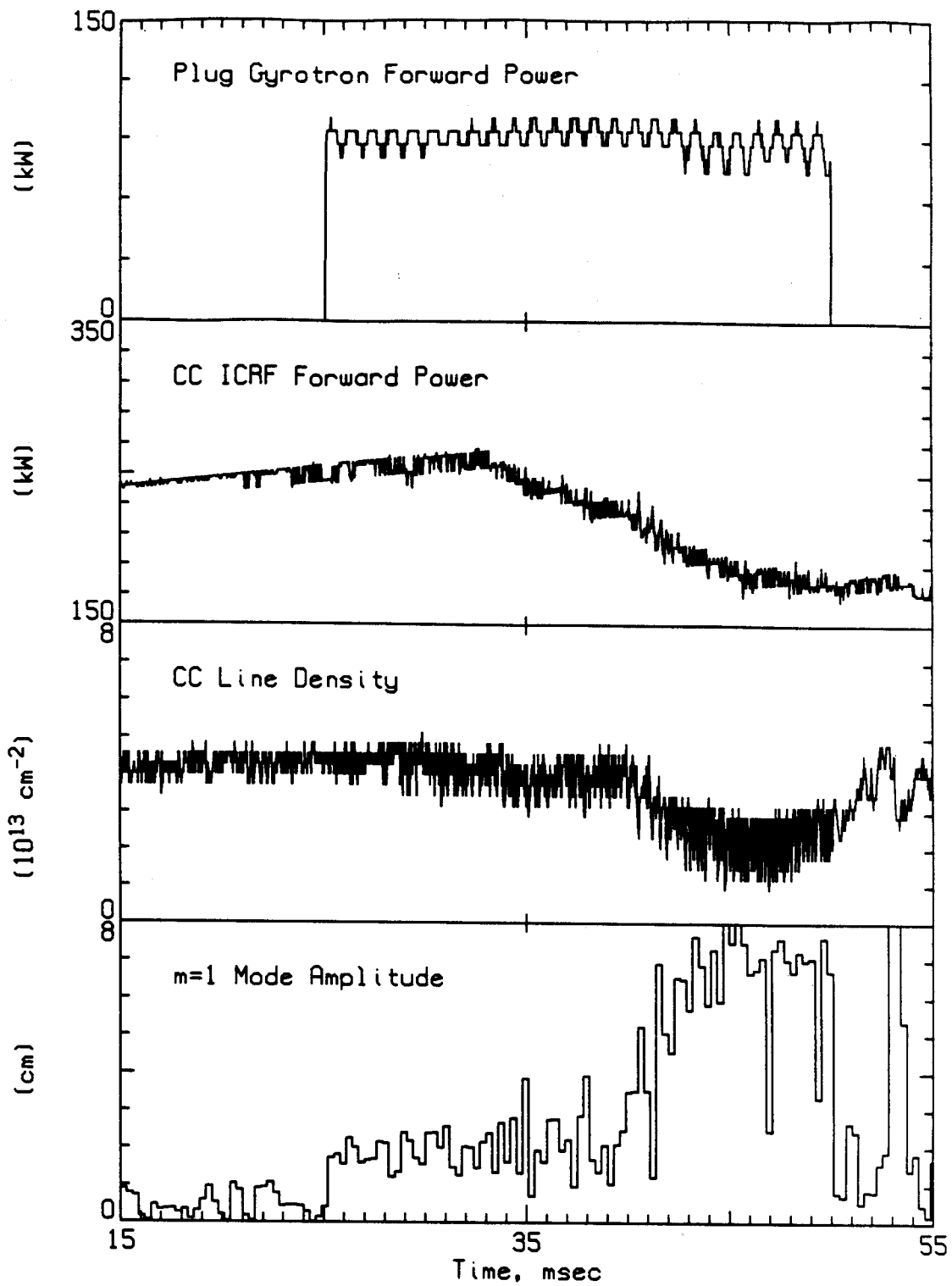


Figure 5. The time history of a plugging instability shot is shown. The large amplitude $m = 1$ fluctuations accompanied by central cell density drop occur during the north plug ECH pulse when the central cell ICH power level drops below the stability boundary.

than the time into the ECH heating pulse. In figure 6, we show the

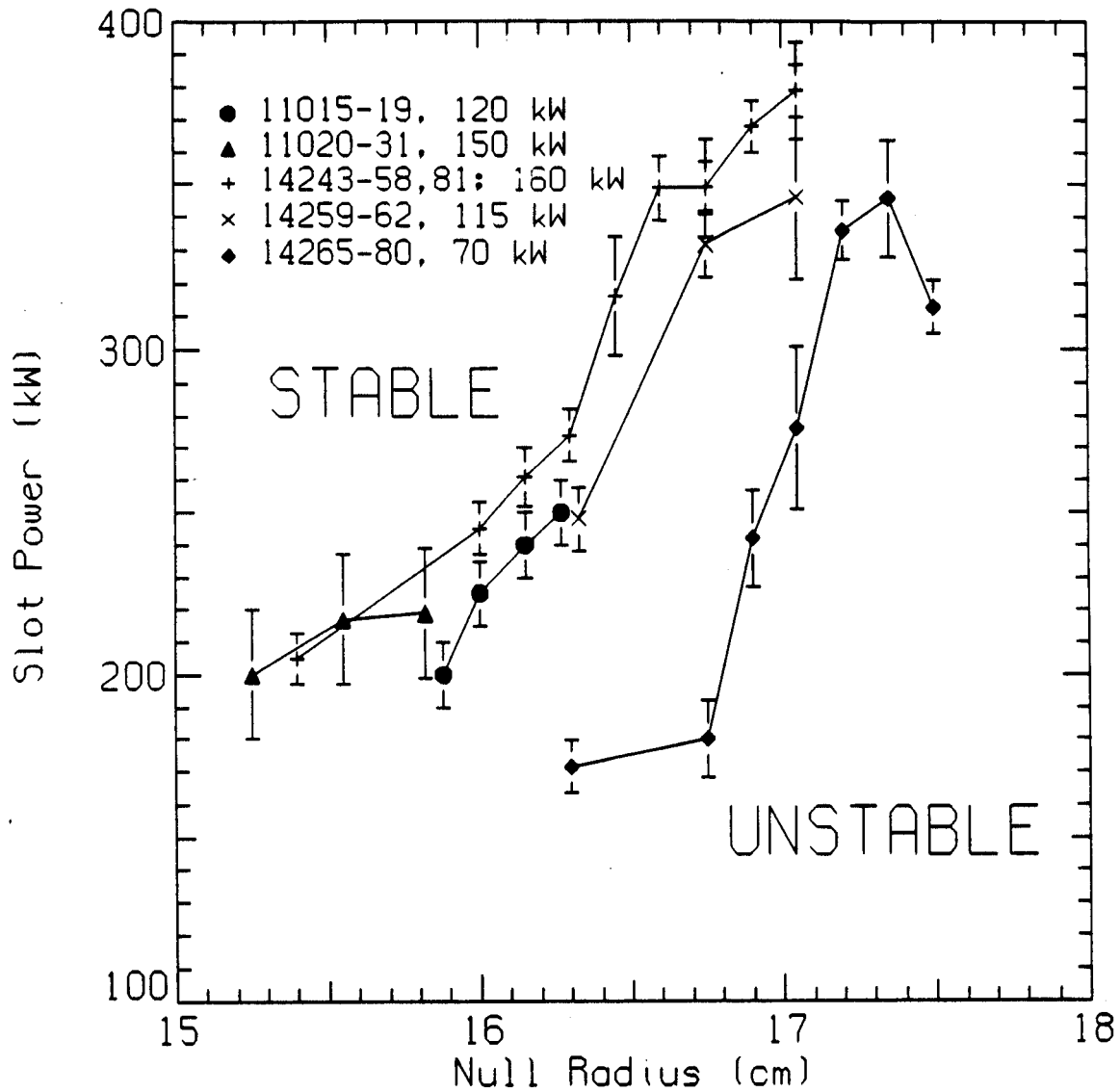


Figure 6. The multi-parameter nature of the stability boundary is shown at constant fueling rate. Plug ECH drives the plasma unstable. Enhanced stability is achieved by mapping the null deeper into the plasma, raising the central cell ICH power level, or both.

stability boundary relative to these two operational parameters for sev-

eral power levels of ECH heating in the axicell. We note that higher ICH power and smaller null radius are stabilizing, while higher ECH power is destabilizing. Figure 6 demonstrates the interplay of divertor and ICH stabilization on two widely separated run days. The scaling of these stability boundaries with divertor current and ICH power is reproducible as shown, however it is serendipitous that the boundaries are unchanged on these two runs.

The parametric dependence of stability on divertor mapping is also characterized by a sharp threshold, as figure 7 illustrates. We plot the amplitude of the coherent $m = 1$ mode versus null radius for fixed ICH power, ECH power, and fueling rate. This parameter scan corresponds to moving along a horizontal line in figure 6 at a slot power level of 175 kW.

The parametric dependence of stability on fueling rate shows a similar threshold. Figure 8 demonstrates the onset of instability as the fueling rate is lowered during axicell ECH heating when the radius of the null is 17.2 cm. This threshold is extended to lower fueling rates as the divertor null is mapped inwards. In this case a stability threshold was encountered between 16 and 18 torr-l/sec. compared to 24 torr-l/sec on subsequent shots with the divertor off. These effective fueling

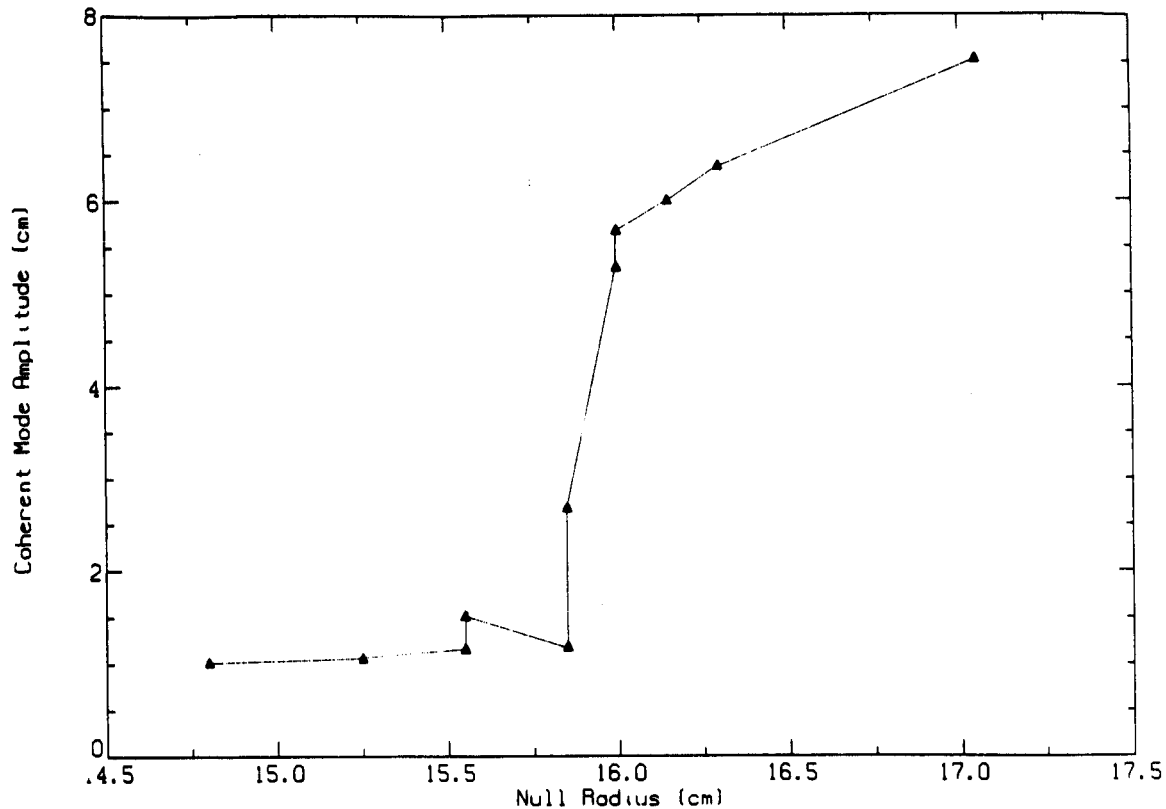


Figure 7. The threshold effect of the divertor stabilization is shown. With the null mapping at or inside the stability boundary, the plasma is stable to the $m = 1$ mode. The fluctuations are plotted as the spatial amplitude of the instability, calculated from the multi-chord interferometer array data.

rates are also dependent on other parameters, such as wall conditions and vacuum quality, thus can change from day to day.

IV – Comparison with Theory and Alternate Mechanisms

The divertor was designed to stabilize via incoherent azimuthal electron drifts in the null. The data presented in section V show that

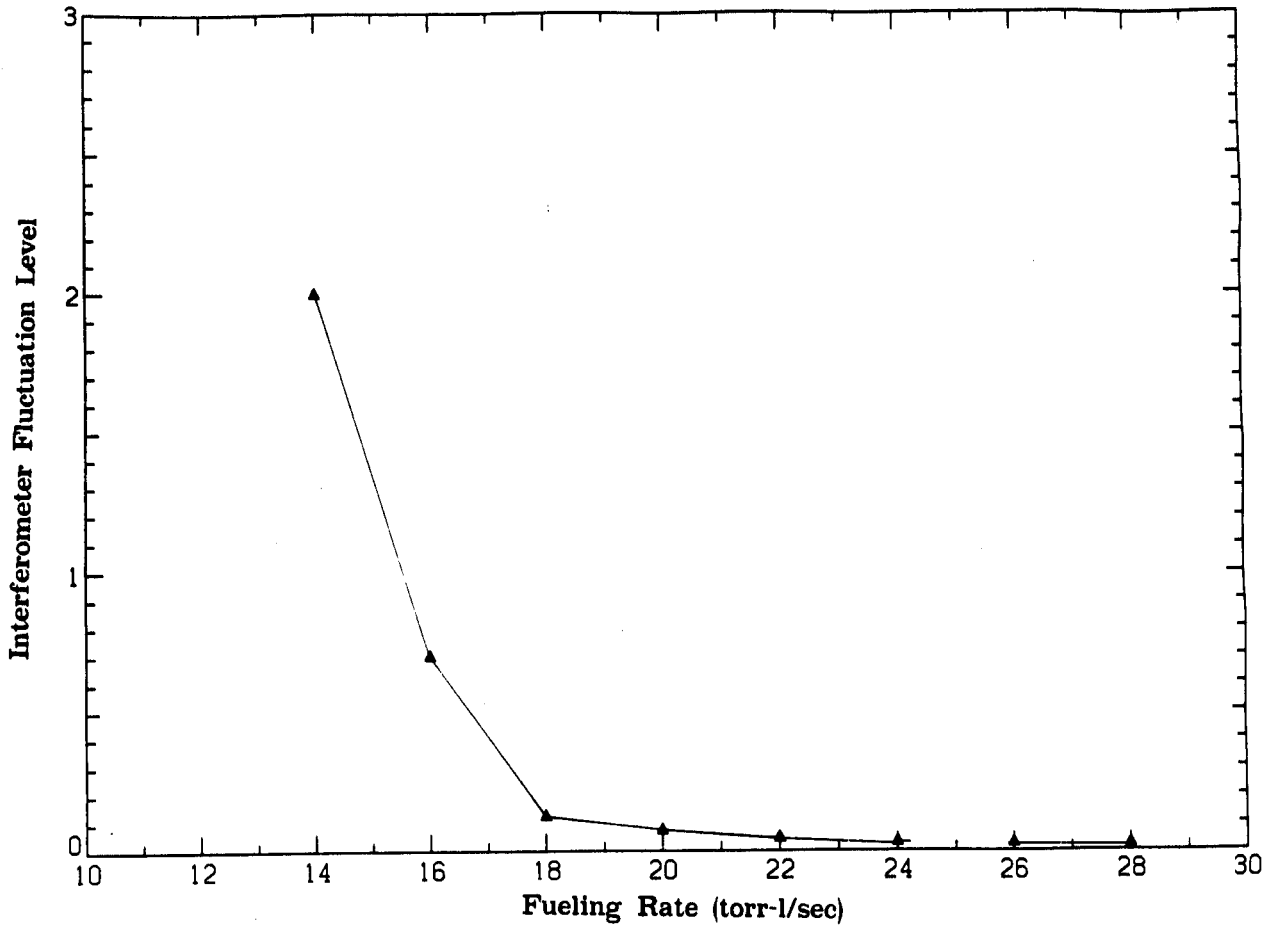


Figure 8. The stability threshold vs. fueling rate is shown. The fluctuation amplitude (shown as $\delta n/n$ for a central cell interferometer) increases dramatically below 18 torr-l/sec fueling rate.

the divertor does extend the parameter range over which the plasma is stable. The technique used to destabilize the plasma, however, does not allow us to quantify the destabilizing drive, or consequently the degree of stabilization provided by the divertor. In this section, we qualitatively examine the possible mechanisms for our positive experimental results. We will first consider a prediction of the proposed theory, and then examine several alternate theories.

A direct result of theory is that MHD fluctuations on the flux surface mapping to the null should be suppressed during divertor operation. Figure 9 shows a radial scan of the heavy-ion-beam-probe (HIBP) in the central cell “well” on a marginally stable shot. The signal is proportional to the diagnostic beam current, plasma density, and a function of electron temperature. The fluctuation amplitude decreases in the vicinity of the null radius. Fourier transforms of the signal shows that although the broadband fluctuations are not affected, the amplitude of the $\mathbf{E} \times \mathbf{B}$ frequency (10 kHz) decreases significantly past the null, in agreement with the model of electron drifts in the null. The lower shot was taken at higher bucking coil current, mapping the null 1.5 cm deeper into the plasma. Although the smaller null radius stabilizes the fluctuations and makes the observation difficult, the same break may be seen.

As an alternative mechanism, we consider the possibility that enhanced compressibility due to the small radius of curvature in the null leads to enhanced stability. Assuming that an MHD model of the plasma is valid, stability can be achieved independent of finite Larmor radius effects if the pressure is of the form

$$P = U^{-\gamma} \quad \text{where} \quad U = \int \frac{dl}{B},$$

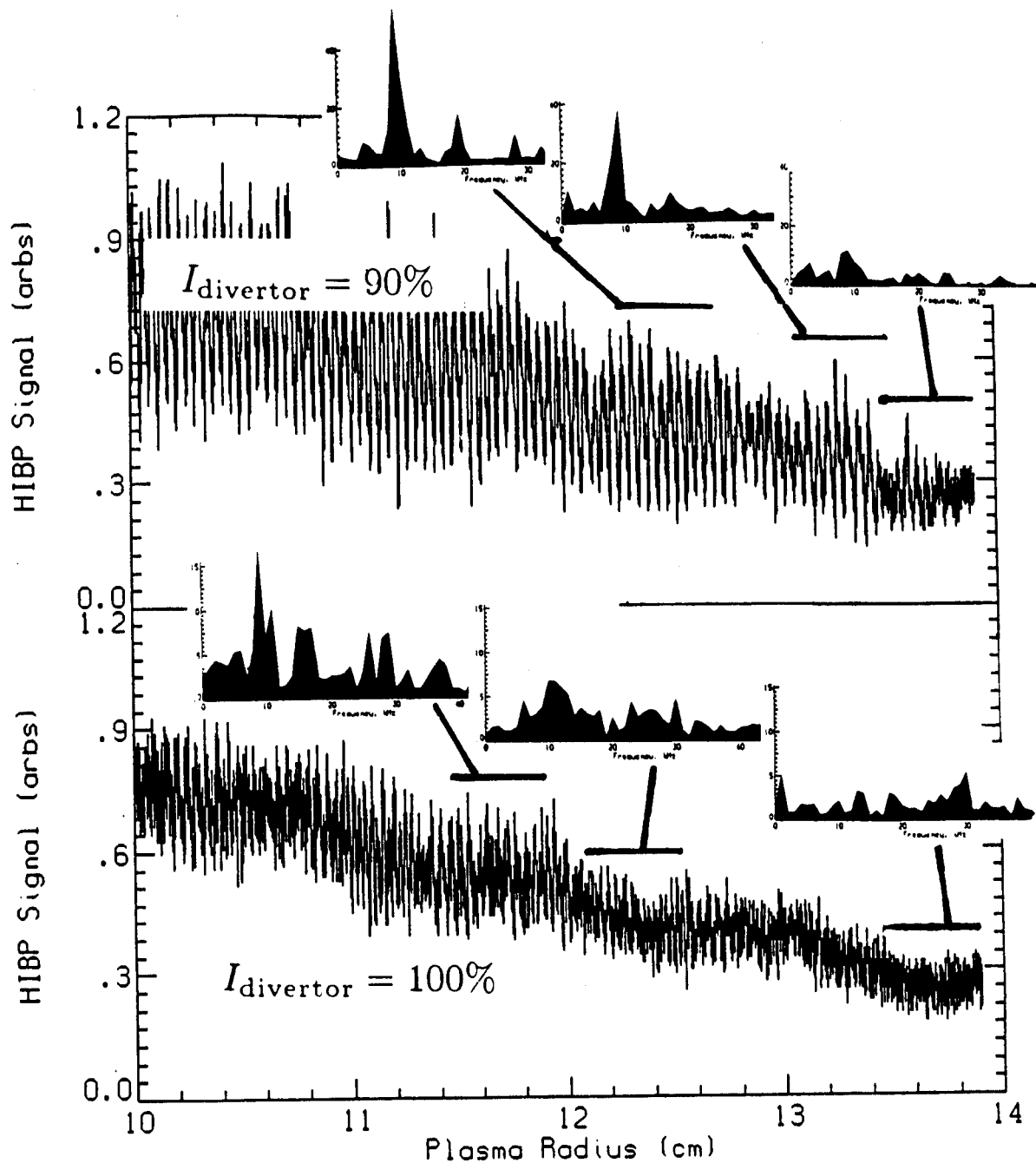


Figure 9. The Heavy-Ion-Beam-Probe (HIBP) shows a point measurement of the plasma density at high time resolution for two different current settings of the bucking coil. In these shots, the radius of the measurement is scanned over 10 msec. The $I_{\text{buck}} = 90\%$ shot is "stable", but very close to the instability threshold. On this shot a clear break in the fluctuation level may be seen at about 13.4 cm. The $I_{\text{buck}} = 100\%$ shot is much more stable — at the higher current, the null maps 1.5 cm deeper into the plasma. A smaller break in fluctuations may be seen on this shot at about 12 cm. Inset Fourier transforms over the windows marked show that the $m = 1$ mode (at about 10 kHz) is suppressed outside the fluctuation breaks. (The 100% shot FFT scales are $3\times$ more sensitive.)

assuming that the pressure is isotropic. This requires a pressure profile which is flat through the core and drops steeply to zero at the null. We are not able to test this by direct measurements of the pressure profile in the null region, but we can infer the density profile from the multichord interferometer array, located 2 m from the null in the central cell “well”. In figure 10, we show statistical fits to the multichord interferometer diagnostic for a representative quiescent shot. Several profiles of varying slope are attempted. We consistently observe that a Gaussian profile yields the best fit. Profiles which are constant through the core with large density gradients on the edge (i.e. $n_e(r) = n_{e0}(1 - (r/r_0)^8)$) are not consistent with the data, and the lower density gradients of a Gaussian profile are inconsistent with the requirements for significant compressibility stabilization. These profiles are also consistent with HIBP radial scans, as in figure 9.

If we include finite Larmor radius effects, the profile requirements for stability are relaxed, but stability requires a large plasma pressure near the null where the curvature is strong. Again, measurements here are difficult, however we may make the following observations. The central cell well plasma is measured to be anisotropic from both scanning charge exchange measurements and diamagnetic loop ratios,

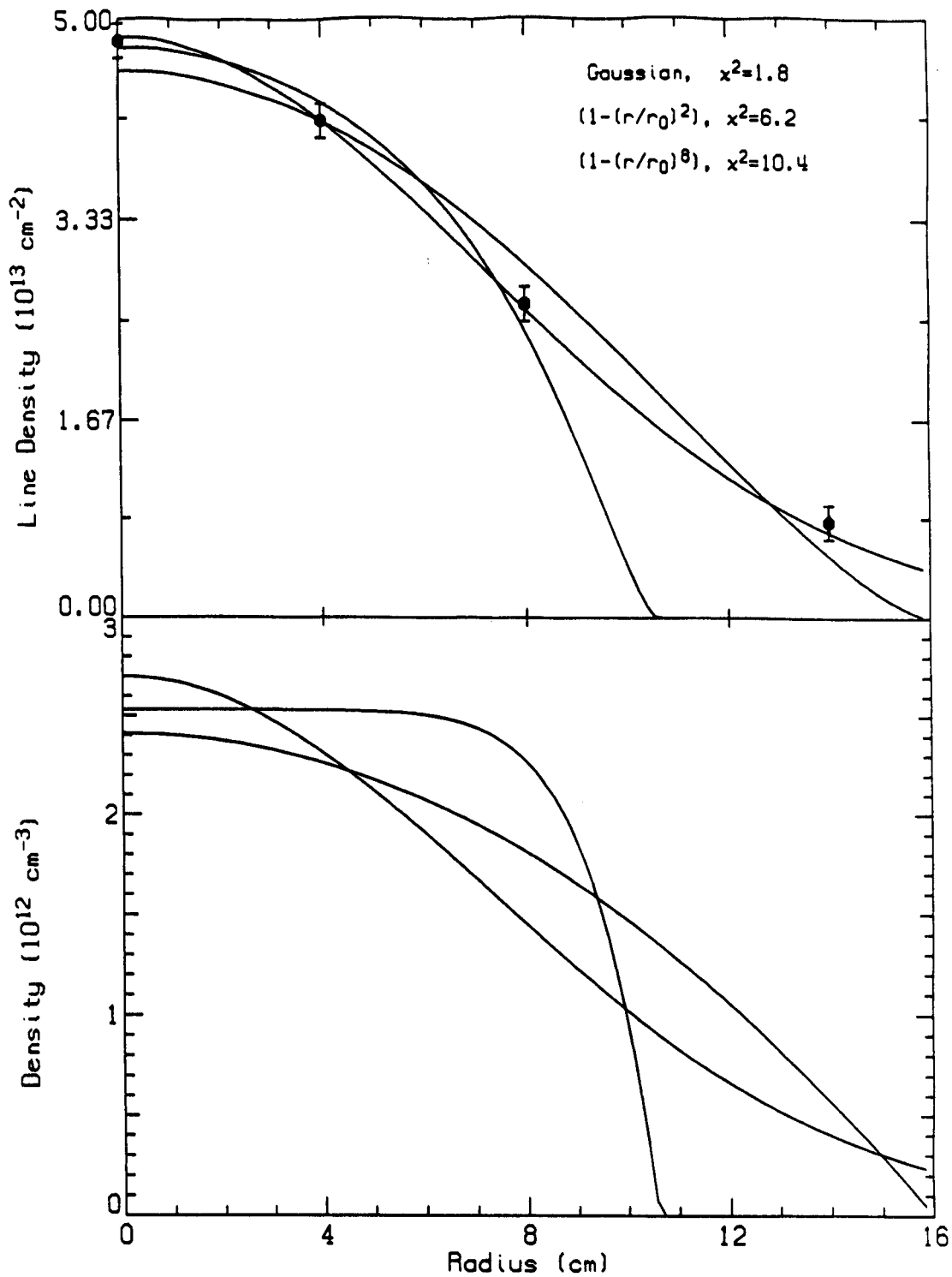


Figure 10. Multi-chord interferometer data is fit to several model profiles during quiescent operation. The "best fit" profiles are shown for 3 of these. Both the density and line-integrated density are shown, with the 4 chords of data overlaid on the line-density fit. The Gaussian profile is clearly best; a consistent result. Flat profiles with high edge gradients, (necessary to explain stabilization results via compressibility and uniformly local stability), are not consistent with measured profiles.

with a ratio of perpendicular to parallel temperature of 4 — 6. Thus the passing ion population near the null has a lower plasma pressure than the plasma confined in the wells. This leaves the possibility that plasma could be locally trapped near the null. The energy source for this plasma is the ICH resonance which forms a torus containing the ring null with a minor radius of 2 cm. Because $\nabla_z \mathbf{B}$ is large at this point, the heating rate is reduced from the heating rate in the well region. The particle loss rate from this region is also high since the ions which pass through the resonance also pass near enough to the null to lose adiabaticity. Finally, the energy loss rate due to charge exchange at this point in the plasma is high. Neutrals are available both from the adjacent gas box and from scrape off on metallic surfaces of the diverted plasma. The plasma density is low at the plasma edge since the null region is beyond the typical $1/e$ density radius and the neutral shielding is poor. We conclude that it would be difficult to sustain a high plasma pressure near the null and that compressibility is probably not the source of stability.

Line-tying^{18,19} on the divertor coils and/or limiters is a possible mechanism for stabilization. Figure 11 shows that grounding the divertor coil housing is necessary for effective stabilization. The likely

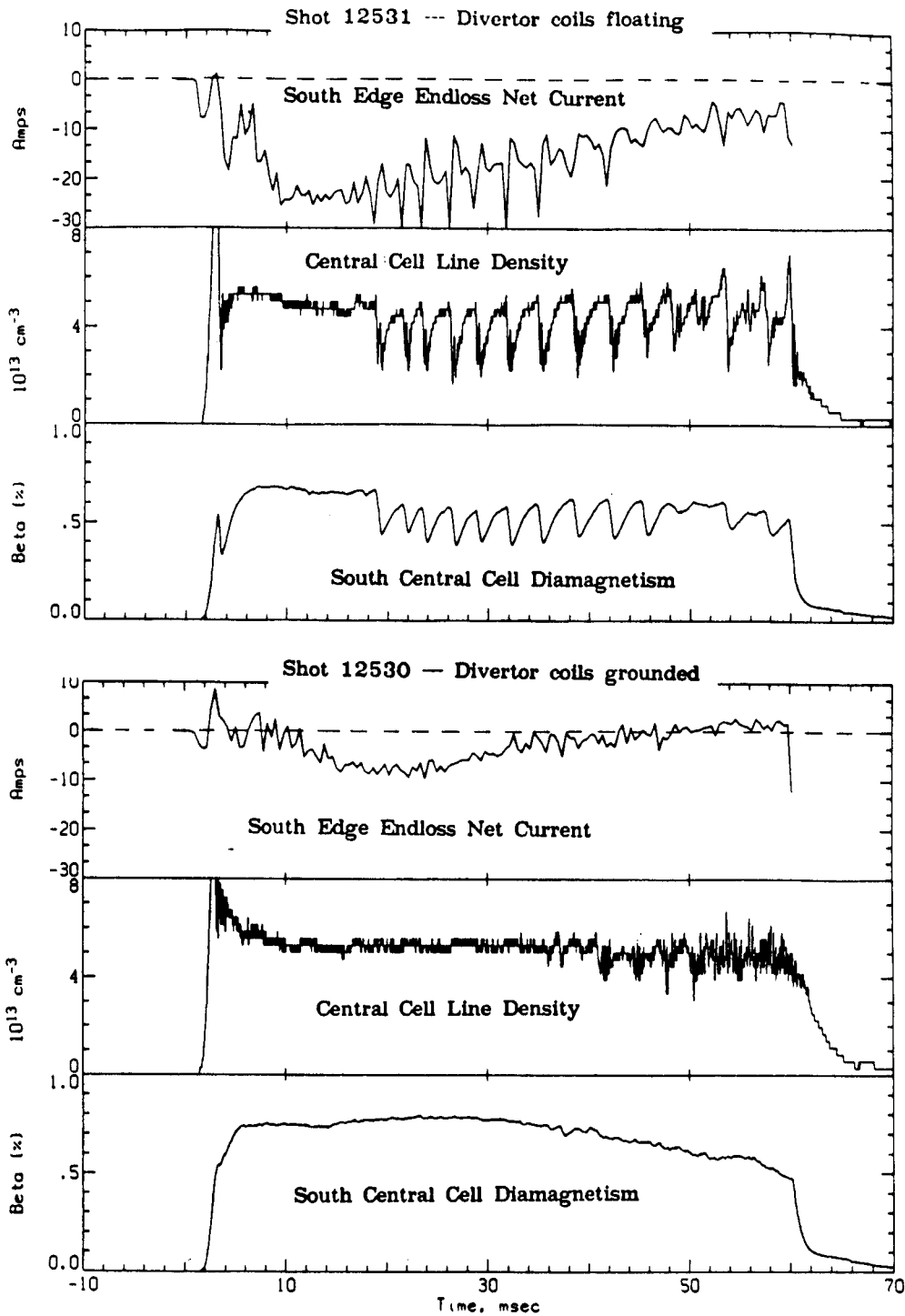


Figure 11. Floating the divertor coils defeats the stabilizing effect of the divertor. Two similar shots were taken with the grounding straps alternately attached and removed from the coils. Subsequent measurements show that only the south small ("boost") coil receives any significant current, collecting about 5 Amps of electron current while grounded during a typical discharge.

mechanism for this would be that scrape-off of plasma on the “boost” coil limiters near the null (figure 2) provides a route for azimuthal current flow much like the null is conjectured to. The stabilizing effect would then scale with divertor current, (as in figures 6 and 7), since the scrape off flux surface would map deeper into the plasma with increasing “bucking” coil current.

In this case, however, the divertor would act as a limiter – and the plasma radius would scale with the divertor current, which it does not. Probe scans in the region of diverted flux (i.e. near the “bucking” coil) show a density profile consistent with magnetic field mapping calculations⁹, also implying that scrape off on the small coil limiters cannot be a serious problem. In addition, the plasma radius characteristically decreases with increasing ICH power¹⁴. If the divertor stabilization were due to line-tying, this scaling would “pull” the plasma away from the limiter as the ICH power increased, and the ICH and divertor stabilization effects would not be additive (as in figure 6).

It is more difficult to assess the effect on the plasma of power losses, (and hence β profile changes), in the diverted flux. Changes in the equilibrium profile may decrease the instability drive or enhance the effect of ponderomotive stabilization²². The strength of the ICH E_z

field, largely responsible for ponderomotive stabilization, is calculated with the ANTENA code²³, which predicts a high sensitivity to profile edge effects (temperature, density, etc). The edge electron temperature profile, however, does not show significant edge cooling at higher divertor currents. The radially scannable central cell Thomson scattering diagnostic²⁴ shows a slightly hollow radial profile (figure 12), which is not markedly affected by raising the divertor field (mapping the null inwards).

VII – Summary

A divertor has been successful in extending the stability limits of $m = 1$ interchange modes in Tara in a purely axisymmetric magnetic field configuration. Stability of non diverted plasmas is limited by thresholds in fueling rate, ICH power, and ECH power; all these limits are extendable with divertor operation. The degree of enhanced stability increases with the current in the divertor bucking coil — thus stability improves as the null is mapped radially inwards in the central cell. In addition, this stability enhancement is additive with ICH induced (ponderomotive) stabilization. Fluctuations at the $\mathbf{E} \times \mathbf{B}$ frequency

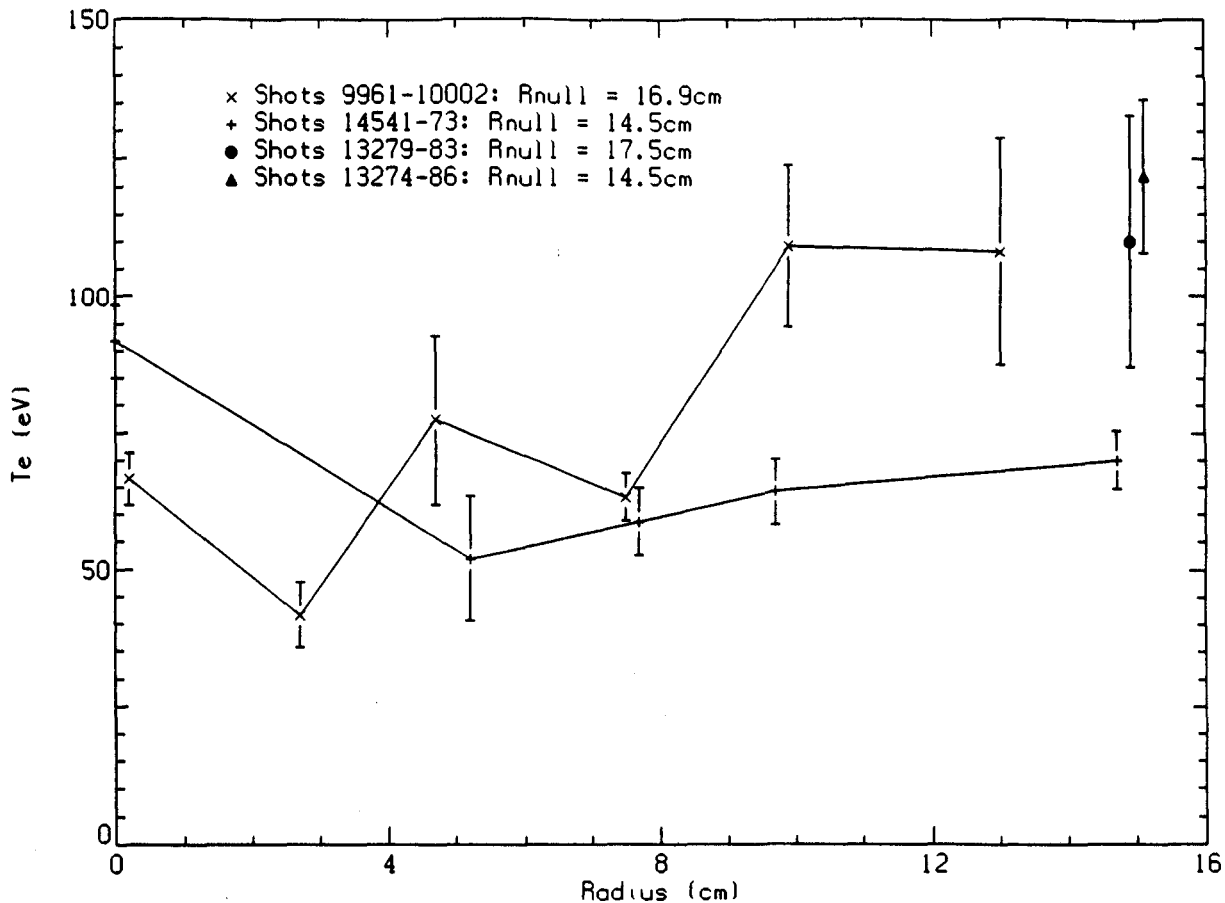


Figure 12. Radially scannable Thomson scattering measurements in the central cell "well" show a slightly hollow profile with no indication of edge cooling at greater divertor fields. Runs taken with the divertor bucking coil set for a null radius of 16.9 cm. versus runs taken at higher current (with the null mapping to 14.5 cm.) show no measurable edge T_e profile change. The outermost radial measurement shows no appreciable edge cooling when mapped outside the null radius.

have been observed to decrease at the null radius, in agreement with theory. Several alternate theoretical mechanisms for divertor stabilization have been discussed; changes in the equilibrium plasma pressure profile due to divertor mapping may also play a role in stabilization.

Acknowledgments

We are pleased to acknowledge valuable conversations with N. Hershkowitz regarding the effects of edge T_e on ponderomotive stabilization, and V. Pastukhov regarding the effects of compressibility on stabilization. We also wish to acknowledge the efforts of M. Olmstead, E. Georgelis, and J. Tarrh in the design of the divertor; and W. Brooks, M. Gaudreau, K. George, R. Rameriz, M. Shuster, W. Stein, and P. Thomas for their technical support. This work was supported by the Department of Energy under contract number DE-AC02-78ET51013.

References:

- ¹J.R. Ferron, A.Y. Wong, G. Dimonte, and B.J. Leikind. *Phys. Fluids* **26**, 2227 (1983)
- ²J.R. Ferron, R. Goulding, B.A. Nelson, T. Intrator, E.Y. Wang, G. Severn, N. Hershkowitz, D. Brouchous, J. Pew, R.A. Breun, and R. Majeski. *Phys. Fluids*, **30** 2855 (1987)
- ³J. Kesner, R.S. Post, B.D. McVey, and D.K. Smith. *Nucl. Fusion* **22**, 549 (1982)
- ⁴R.S. Post, M. Gerver, J. Kesner, J.H. Irby, and B.G. Lane, *Plasma Physics and Controlled Nuclear Fusion Research*, 1984, London, United Kingdom (IAEA, Vienna, 1985), Vol II, p. 285.
- ⁵T.C. Simonen, S.L. Allen, D.E. Baldwin, T.A. Casper, J.F. Clauser, F.H. Coensgen, R.H. Cohen, D.L. Correll, W.F. Cummins, C.C. Damm, J.H. Foote, T.K. Fowler, R.F. Goodman, D.P. Grubb, D.N. Hill, E.B. Hooper, R.S. Hornady, A.L. Hunt, R.G. Kerr, G.W. Leppelmeier, J. Marilleau, J.M. Moller, A.W. Molvik, W.E. Nexsen, J.E. Osher, W.L. Pickles, P. Poulsen, G.D. Porter, E.H. Silver, B.W. Stallard, J. Taska, W.C. Turner, J.D. Barter, T.W. Christensen, G. Dimonte, T.E. Romesser, R.F. Ellis, R.A. James, C.J. Lasnier, T.L. Yu, L.V. Berzins, M.R. Carter, C.A. Clower, B.H. Failor, S. Falabella, M. Flammer, T. Nash, and W.L. Hsu, *Plasma Physics and Controlled Nuclear Fusion Research*, 1984, London, United Kingdom (IAEA, Vienna, 1985), Vol. II, p. 255.
- ⁶N. Hershkowitz, R.A. Breun, D.A. Brouchous, J.D. Callen, C. Chan, J.R. Conrad, J.R. Ferron, S.N. Golovato, R. Goulding, S. Horne, S. Kidwell, B. Nelson, H. Persing, J. Pew, S. Ross, G. Severn, and D. Sing, *Plasma Physics and Controlled Nuclear Fusion Research*, 1984, London, United Kingdom (IAEA, Vienna, 1985), Vol. II, p. 265.
- ⁷S. Miyoshi, T. Cho, M. Ichimura, M. Inutake, K. Ishii, A. Itakura, I. Katanuma, T. Kawabe, Y. Kiwamoto, A. Mase, Y. Nakashima, T. Saito, K. Sawada, D. Tsubouchi, N. Yamaguchi, and K. Yatsu, *Plasma Physics and Controlled Nuclear Fusion Research*, 1984, London, United Kingdom (IAEA, Vienna, 1985), Vol. II, p. 275.

⁸D.D. Ryutov and G.V. Stupakov, *JETP Lett.* **26**, 174 (1977); R.H. Cohen. *Nucl. Fusion*, **19** 1579 (1979)

⁹J.A. Casey, B.G. Lane, J. Kesner, and R.S. Post. *Bull. Amer. Phys. Soc.*, **31**, 1424 (1986)

¹⁰R.S. Post, K. Brau, J. Casey, J. Coleman, S. Golovato, W. Guss, S. Horne, J. Irby, J. Kesner, B. Lane, M. Mauel, L. Pócs, E. Sevillano, D. Smith, J. Sullivan, and R. Torti, *J. Nuclear Materials*, 145-147 (1986) 81-86

¹¹B. Lane, R.S. Post, and J. Kesner. *Nucl. Fusion* **27**, 277 (1987)

¹²B. Lane, J. Kesner, R.S. Post, and J.A. Casey. *Bull. Amer. Phys. Soc.*, **31**, 1424 (1986)

¹³J.H. Irby, B.G. Lane, J.A. Casey, K. Brau, S.N. Golovato, W.C. Guss, S.F. Horne, J. Kesner, R.S. Post, E. Sevillano, J.D. Sullivan, and D.K. Smith. (Accepted for publication by *Phys. Fluids*.)

¹⁴S.N. Golovato, D.K. Smith, K. Brau, J. Casey, W. Guss, S. Horne, J. Irby, J. Kesner, B. Lane, R. Myer, R.S. Post, E. Sevillano, J. Sullivan, and R. Torti, *Bull. Amer. Phys. Soc.*, **31**, 1423 (1986)

¹⁵R.S. Post, K. Brau, S. Golovato, E. Sevillano, D.K. Smith, W. Guss, J. Irby, R. Myer, and J. Sullivan. *Nuclear Fusion*, **27**, 217 (1987)

¹⁶M.N. Rosenbluth and C.L. Longmire. *Annals of Physics*, **1**, 120 (1957)

¹⁷V.P. Nagorny and G.V. Stupakov. *Sov. J. Plasma Phys* **10**, 275 (1984)

¹⁸M. Vuillemin, *Nucl. Fusion Suppl.* Part I, 341 (1962)

¹⁹W.B. Kunkel and J.U. Guillory, in *Proceedings of the Seventh Conference on Phenomena in Ionized Gases*, Belgrade, 1965, edited by B. Perovic and D. Tocsic, Vol. II, p. 702.

²⁰J.A. Casey, E. Sevillano, J.H. Irby, and B.G. Lane. MIT-PFC/JA-87-26 (1987). Submitted to *Rev. Sci. Instrum.*

²¹J.R. Myra and D.A. D'Ippolito. *Phys. Rev. Lett.* **53**, 914 (1984); D.A. D'Ippolito and J.R. Myra. *Phys. Fluids*, **28** 1895 (1985); J.R.

Myra and D.A. D'Ippolito. *Nuclear Fusion*, **26** 361 (1986); D.A. D'Ippolito and J.R. Myra. *Phys. Fluids*, **29** 2594 (1986)

²²C. Litwin and N. Hershkowitz. *Phys. Fluids*, **30** 1323 (1987)

²³See National Technical Information Service Document No. DE85004960 ("ICRF Antenna Coupling Theory for Cylindrically Stratified Plasma," Massachusetts Institute of Technology report PFC/RR-84-12 by B. McVey). Copies may be ordered from the National Technical Information Service, Springfield, Virginia 22161. The price is \$16.95 plus a \$3.00 handling fee. All orders must be prepaid.

²⁴J.A. Casey and J.H. Irby, *Rev. Sci. Instrum*, **57**, 1804 (1906)